Transient Strain Driven by a Dense Electron-Hole Plasma

M. F. DeCamp,[1] D. A. Reis,[1] A. Cavalieri,[1] P. H. Bucksbaum,[1] R. Clarke,[1] R. Merlin,[1] E. M. Dufresne,[1] D. A. Arms,[1] A. M. Lindenberg,[2] A. G. MacPhee,[2] Z. Chang,[3] B. Lings,[4] J. S. Wark,[4] and S. Fahy[5]

[1]*FOCUS Center and Department of Physics, University of Michigan, Ann Arbor, Michigan 48109, USA*
[2]*Department of Physics, University of California, Berkeley, California 98720, USA*
[3]*Department of Physics, Kansas State University, Manhattan, Kansas 66506, USA*
[4]*Department of Physics, Clarendon Laboratory, University of Oxford, Oxford, OX1 3PU, United Kingdom*
[5]*Physics Department and NMRC, University College, Cork, Ireland*

(Received 31 December 2002; published 16 October 2003)

We measure transient strain in ultrafast laser-excited Ge by time-resolved x-ray anomalous transmission. The development of the coherent strain pulse is dominated by rapid ambipolar diffusion. This pulse extends considerably longer than the laser penetration depth because the plasma initially propagates faster than the acoustic modes. X-ray diffraction simulations are in agreement with the observed dynamics.

DOI: 10.1103/PhysRevLett.91.165502 PACS numbers: 63.20.–e, 42.65.Re, 61.10.Nz

Subpicosecond laser-induced electron-hole plasmas in semiconductors can produce large amplitude lattice strain and rapid loss of translational order. These effects have been studied extensively in ultrafast linear and nonlinear reflectivity experiments [1–8] and, more recently, in time-resolved x-ray Bragg scattering experiments [9–15]. X-ray diffraction has the advantage that it can provide quantitative structural information.

Ultrafast strain propagation was recently used to control the time-resolved anomalous transmission of x rays [16]. The current work uses this new technique as a bulk sensitive structural probe to study the long-standing problem of propagation and coupling to the lattice of a dense electron-hole plasma following laser excitation.

Many previous x-ray experiments [9,10,15] have been analyzed using the thermoelastic model put forward by Thomsen *et al.* [17,18] in which the strain is caused by differential thermal expansion. Deviations from this model are discussed in Thomsen *et al.* and have been seen with x-ray diffraction [10,12,13,15,16]. In particular, Cavalleri *et al.* [12,13] studied coherent strain near the melting threshold in Ge utilizing x-ray Bragg diffraction. They concluded that the strain is produced over a region which is thick compared to the optical penetration depth, likely due to ambipolar diffusion. However, their experiment was sensitive only to structural changes in the near surface region due to the short x-ray extinction depth.

In the present experiments, the laser intensity is sufficient to impulsively generate a dense electron-hole plasma at the crystal surface, the dynamics of which are governed by ambipolar diffusion [19] and Auger recombination. The plasma couples to the lattice through the deformation potential. Because the electron-hole plasma diffusion is not limited by the sound speed of the material, the strain *front* initially advances faster than the sound speed. The resulting acoustic pulse travels into the crystal bulk at the longitudinal sound speed.

In order to probe the resulting coherent acoustic pulse as it travels deep within the bulk, we utilize the Laue geometry whereby two linearly independent wave solutions (α and β) propagate through the crystal. Transverse to the propagation, these two solutions are standing waves whose wavelengths are twice the spacing of the diffracting planes. The solutions are labeled α and β with the convention that α has its nodes, and β its antinodes on the diffracting planes. In the case that all atoms lie on these planes, α is maximally transmitted and β is maximally absorbed. Because the two solutions interact with different electron densities, they propagate with different velocities.

Emerging from the crystal are two diffracted beams: one in the direction of the input beam (forward-diffracted or "0" beam), and the other in the direction determined by the vector sum $\vec{k}_H = \vec{k}_0 + \vec{G}_H$ (deflected-diffracted or H beam). Here $\vec{k}_0$ ($\vec{k}_H$) corresponds to the wave vector of the forward-diffracted (deflected-diffracted) beam and $\vec{G}_H$ is the reciprocal lattice vector corresponding to the diffracting planes. These beams are linear combinations of α and β. Their intensities are given by

$$I_0 = |a\vec{E}_\alpha e^{i\vec{k}_\alpha\cdot\vec{z}} + b\vec{E}_\beta e^{i\vec{k}_\beta\cdot\vec{z}}|^2, \quad (1)$$

$$I_H = |c\vec{E}_\alpha e^{i\vec{k}_\alpha\cdot\vec{z}} - d\vec{E}_\beta e^{i\vec{k}_\beta\cdot\vec{z}}|^2, \quad (2)$$

where $\vec{E}_{\alpha,\beta}$ is the field amplitude inside the crystal, $\vec{k}_{\alpha,\beta}$ is the complex wave vector of the α, β solutions (including absorption), and a, b, c, d are determined by the crystal orientation. The two modes α and β oscillate in and out of phase as they propagate through the crystal. The wavelength of the interference, $\Lambda = |\vec{k}_\alpha - \vec{k}_\beta|^{-1}$, is known as the Pendellösung length which is typically a few to tens of microns and is often shorter than the absorption length.

For a crystal that is thick compared to the β-absorption length, only the α solution survives and there is no interference. This is the anomalous transmission of x rays,

known as the Borrmann effect [20]. A distortion of the lattice can cause a redistribution of the interior wave solutions [21]. Figure 1 shows the effect of a thin region of distortion regenerating the β solution after it has decayed away in a thick crystal for the case of zero α absorption. When this occurs close enough to the crystal exit, the regenerated β wave does not decay away and interference occurs at the exit face, despite the fact that the crystal is thick.

A short acoustic pulse can be considered as a moving lattice disturbance. We have recently shown that such a pulse can be used to coherently transfer energy between the two diffracted beams [16]. Following an initial transient, the diffracted x-ray intensities oscillate in time as the pulse travels into the crystal bulk with a period that is given by the Pendellösung length divided by the speed of sound. In this Letter, we focus on the physics of strain generation as a function of incident laser fluence. Deviations from impulsive strain generation are evident in the relative phase of the oscillations and the amplitude of the transient, providing information about the strain generation process at times shorter than the x-ray probe duration.

The experiments were performed at the 7-ID undulator beam line at the Advanced Photon Source. The x-ray energy was set to 10 keV using a cryogenically cooled Si 111 double crystal monochromator leading to a 1.4×10^{-4} fractional energy spread. The x-ray beam is masked by tantalum slits to ensure that the x-ray spot is smaller than the laser spot on the sample and to provide x-ray collimation. The sample is a 280 μm thick, (001) Ge single crystal. The crystal was oriented such that the x rays diffracted in the asymmetric $20\bar{2}$ Laue geometry. In this geometry, and at 10 keV, the Pendellösung length is 6.2 μm and the β absorption length is 19 μm, normal to the surface. Therefore, in the unperturbed crystal, essentially only α survives at the exit. The only significant difference between the two diffracted beams is in their direction and a mismatch in their amplitudes due to details of the boundary conditions on the exit face [20].

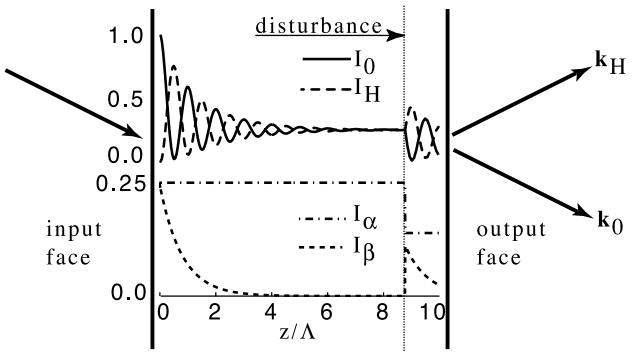

FIG. 1. Intensities of the forward- and deflected-diffracted beams (upper) and the interior solutions α, β (lower) as a function of depth inside a thick crystal. A lattice disturbance near the exit couples the two solutions, regenerating β.

Coherent strain pulses are produced on the x-ray output face of the crystal by sub-100 fs, 800 nm laser pulses (1 kHz repetition rate) focused to a 1.5 mm^2 spot on the crystal surface. The incident laser fluence was controlled by using a wave plate/polarizer pair prior to focusing and was kept below the observed damage threshold. The resultant excitation is fully reversible in the sense that the time between laser pulses is sufficient to reestablish thermal equilibrium. The laser is phase locked to the x-ray beam to better than the x-ray pulse duration. The laser is timed to the x rays using a combination of a digital delay generator and an electronic phase shifter in the phase-locked loop. In this manner, the pump-probe delay may be set across a range of ± 1 ms with 19 ps precision. A fast silicon avalanche photodiode (APD) and a picosecond x-ray streak camera [22] were used as the time-resolved detectors. The APD sampled the deflected-diffracted beam intensity and the streak camera sampled the forward-diffracted beam (see Fig. 2). The x-ray bunch separation was $\sim$152 ns, large enough to allow electronic gating and measurement of a single x-ray pulse.

Following laser excitation, high contrast oscillations are observed in the pump-probe data over a large span of excitation densities. Figure 3(a) shows these oscillations in the deflected-diffracted beam. The period of oscillation agrees with the Pendellösung length divided by the longitudinal speed of sound. Assuming a reflectivity of 50% [6], the peak carrier density corresponds to $\sim 3 \times 10^{21}$ cm^{-3} at an incident fluence of 35 mJ/cm^2. At this fluence, the behavior near $t = 0$ shows a large transient that is unresolved with the 100 ps x-ray probe beam. After the transient, the oscillations show a significant phase shift with respect to oscillations that occur following an excitation of 2 mJ/cm^2. The amplitude and frequency of the oscillations are relatively insensitive to the fluence. However, as shown in Fig. 4(a), the phase is strongly dependent on the fluence and is correlated with the amplitude of the initial transient. The relative phase of the oscillation was defined with respect to the 2 mJ/cm^2 excitation and was retrieved from a least squares fit [23,24]. The amplitude of the transient is set by the diffracted intensity at a delay of 200 ps. Most of the energy transfer occurs in $\sim$40 ps, measured with the forward-diffracted beam using a streak camera [see the inset of Fig. 3(a)]. At relatively high fluences (>10 mJ/cm^2), the intensity of the deflected-diffracted beam approximately doubles while the

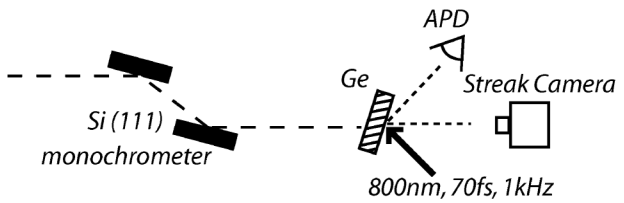

FIG. 2. Experimental setup.

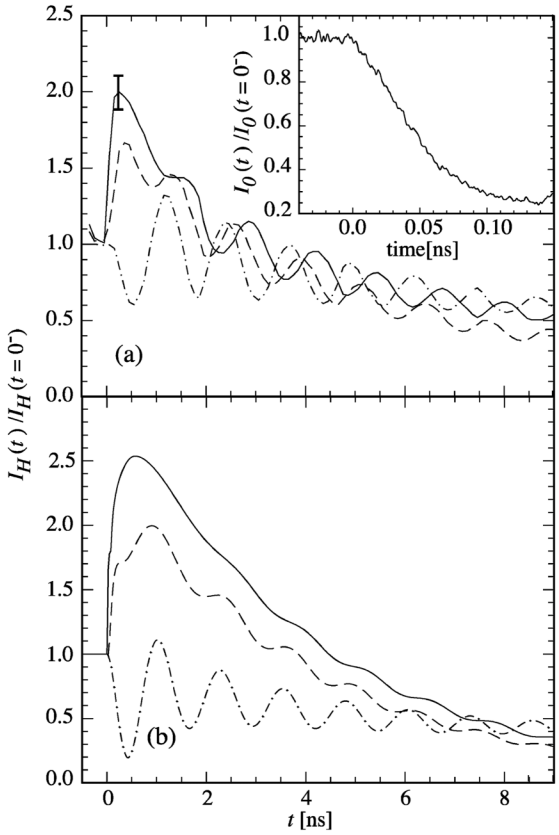

FIG. 3. Time-resolved anomalous transmission. (a) Experiment: Deflected-diffracted intensity for an incident laser fluence of 35 (solid line), 7 (dashed line), and 2 mJ/cm^2 (dot-dashed line). The error bar represents the estimated systematic error in the overall scale. Inset: Streak camera data showing the intensity of the forward-diffracted beam with picosecond resolution at an incident optical fluence of 35 mJ/cm^2. (b) Simulation: Deflected-diffracted intensity for an incident laser fluence of 36 (solid line), 8 (dashed line), and 2 mJ/cm^2 (dot-dashed line).

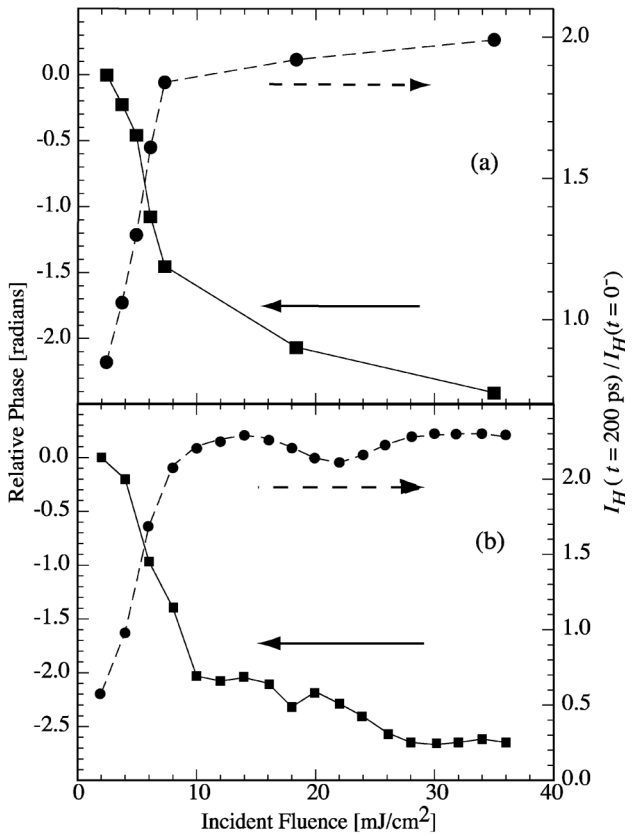

FIG. 4. (a) Experiment: The relative phase of the Pendellösung oscillations (squares) and the normalized deflected-diffracted intensity at a time delay of 200 ps (circles) as a function of incident optical fluence. (b) Simulation: The calculated relative phase of the Pendellösung oscillations (squares) and the calculated normalized deflected-diffracted intensity at a time delay of 200 ps (circles) as a function of incident optical fluence.

forward-diffracted beam is cut by more than 75%. At relatively low fluences (<2 mJ/cm^2), there is no transient.

Inspection of (1) and (2) shows that the maximum energy transfer between the forward and deflected beams near the exit of a thick crystal occurs if the α and β solutions are coupled at a depth of $\Lambda/4$. This implies that the transient behavior is due to a perturbation to the lattice that reaches a depth of more than 1.5 μm into the bulk. In the simplified picture that a moving interface couples the α and β solutions, the excitation must propagate into the bulk at greater than 37 000 m/s, more than 7 times the longitudinal speed of sound.

The strain pulse has a finite spatial extent and is comprised of a spectrum of phonons with different wave vectors. We expect that the phonon component with wavelength equal to the Pendellösung length will resonantly couple the two interior wave solutions [25]. To model this phenomenon, we solve the equations of dynamical diffraction within the crystal, taking into account the laser-induced time-dependent strain profiles, using the Takagi-Taupin formalism adapted for Laue geometry [26,27]. In this method, the differential equations coupling the α and β branches are solved numerically by dividing the crystal into a series of layers of equal thickness. The diffraction intensity of a given lamella is given explicitly in the work of Zachariasen [28]. The depth-dependent strain profile for a given time is taken into account by noting that local strain is equivalent to a change in the local Bragg angle for a given lamella [26,27].

Pure thermoelastic models of strain generation do not predict the observed fluence dependence of the phase and amplitude of the Pendellösung oscillations. A proper model must include the effects of the coupling of the photoexcited plasma to the crystal lattice. We assume that the hot electrons equilibrate with the lattice almost instantaneously. The plasma diffusion is governed by the carrier diffusion and Auger recombination:

$$\frac{\partial n}{\partial t} = D_p \frac{\partial^2 n}{\partial z^2} - An^3, \tag{3}$$

where $D_p = 65\ \mathrm{cm}^2/\mathrm{s}$ is the diffusion constant [29], n is the carrier density which initially follows the laser penetration depth, and $A = 0.11\times10^{-30}\ \mathrm{cm}^6/\mathrm{s}$ is the Auger recombination rate. The evolution of the temperature profile is then governed by carrier and thermal diffusion and the Auger recombination rate:

$$\frac{\partial T}{\partial t} = D_t \frac{\partial^2 T}{\partial z^2} + An^3 \frac{E_g}{C_l}, \tag{4}$$

where $D_t = 0.35\ \mathrm{cm}^2/\mathrm{s}$ is the thermal diffusion constant, $E_g = 0.67\ \mathrm{eV}$ is the electronic band gap, and $C_l = 1.7\ \mathrm{J/K\,cm}^3$ is the crystalline heat capacity.

To calculate the time-dependent strain profile, we use the fact that the equilibrium lattice condition depends on the temperature and the plasma density:

$$\eta(z, t) = \alpha_t T(z, t) + \alpha_p n(z, t), \tag{5}$$

where η is the strain and where $\alpha_t = 10^{-5}\ \mathrm{K}^{-1}$ and $\alpha_p = 0.0013\times10^{-21}\ \mathrm{cm}^3$ are coupling constants for the temperature and plasma components, respectively. In the absence of diffusion, a bipolar pulse develops in the time given by the optical penetration depth divided by the speed of sound [18]. For LA phonons with wave vectors along [100] and a 0.2 μm optical penetration depth, this corresponds to ~40 ps. Including diffusion, the electron-hole plasma extends ~1 μm in the same time, leading to a strain front that has propagated into the bulk faster than the speed of sound.

Figure 3(b) shows the calculated diffraction intensity as a function of laser delay. The sharp initial rise in diffraction intensity is reproduced, as well as the frequency of the time-resolved Pendellösung oscillations. Differences in the absolute phase and depth of modulation, most prevalent at the highest fluences, may be due to imprecise knowledge of the experimental resolution. Nonetheless, the retrieved amplitude and relative phase of the calculated diffracted intensity shows excellent agreement with the data, shown in Fig. 4(b).

In conclusion, we have demonstrated a bulk sensitive probe of lattice dynamics using time-resolved x-ray anomalous transmission. We have observed that electron-phonon coupling modified by carrier diffusion is a dominant mechanism for energy transport in laser-excited Ge. This work could be extended to study how the elastic response of the material can modify the electronic transport properties of semiconductors.

We thank Bernhard Adams, Marcus Hertlein, Don Walko, and Jared Wahlstrand for technical assistance and stimulating discussions. We also thank Jin Wang for use of the intensified CCD camera. This work was conducted at the MHATT-CAT insertion device beam line at the Advanced Photon Source and was supported in part by the U.S. Department of Energy, Grants No. DE-FG02-03ER46023 and No. DE-FG02-00ER15031, by the AFOSR under Contract No. F49620-00-1-0328 through the MURI program, and from the NSF FOCUS physics frontier center. One of us (S. F.) acknowledges the financial support of Science Foundation Ireland. Use of the Advanced Photon Source was supported by the U.S. Department of Energy Basic Energy Sciences, Office of Energy Research, under Contract No. W-31-109-Eng-38.

[1] C.V. Shank and D H. Auston, Phys. Rev. Lett. **32**, 1120 (1974).
[2] C.V. Shank, R. Yen, and C. Hirlimann, Phys. Rev. Lett. **51**, 900 (1983).
[3] H.W. K. Tom, G. D. Aumiller, and C. H. Brito-Cruz, Phys. Rev. Lett. **60**, 1438 (1988).
[4] K. Sokolowski-Tinten, J. Bialkowski, and D. von der Linde, Phys. Rev. B **51**, 14 186 (1995).
[5] K. Sokolowski-Tinten *et al.*, Phys. Rev. B **58**, R11 805 (1998).
[6] K. Sokolowski-Tinten, A. Cavalleri, and D. von der Linde, Appl. Phys. A **69**, 577 (1999).
[7] N.V. Chigarev *et al.*, Phys. Rev. B **61**, 15 837 (2000).
[8] O. B. Wright *et al.*, Phys. Rev. B **64**, 081202 (2001).
[9] C. Rose-Petruck *et al.*, Nature (London) **398**, 310 (1999).
[10] A. M. Lindenberg *et al.*, Phys. Rev. Lett. **84**, 111 (2000).
[11] C. Siders *et al.*, Science **286**, 1340 (1999).
[12] A. Cavalleri *et al.*, Phys. Rev. Lett. **85**, 586 (2000).
[13] A. Cavalleri *et al.*, Phys. Rev. B **63**, 193306 (2001).
[14] K. Solokolowski-Tinten *et al.*, Phys. Rev. Lett. **87**, 225701 (2001).
[15] D. A. Reis *et al.*, Phys. Rev. Lett. **86**, 3072 (2001).
[16] M. F. DeCamp *et al.*, Nature (London) **413**, 825 (2001).
[17] C. Thomsen *et al.*, Phys. Rev. Lett. **53**, 989 (1984).
[18] C. Thomsen *et al.*, Phys. Rev. B **34**, 4129 (1986).
[19] J. Young and H. van Driel, Phys. Rev. B **26**, 2147 (1982).
[20] B. Batterman and H. Cole, Rev. Mod. Phys. **36**, 681 (1964).
[21] *X-ray and Neutron Dynamical Diffraction: Theory and Applications*, edited by A. Authier, S. Lagomarsino, and B. Tanner, NATO ASI Series B (Plenum, New York, 1996).
[22] Z. Chang *et al.*, Appl. Phys. Lett. **69**, 133 (1996).
[23] H. Barkhuijsen *et al.*, J. Magn. Reson. **61**, 465 (1985).
[24] F.W. Wise, M. J. Rosker, G. L. Millhauser, and C. L. Tang, IEEE J. Quantum Electron. **23**, 1116 (1987).
[25] I. R. Entin *et al.*, Sov. Phys. Solid State **20**, 754 (1978).
[26] S. Takagi, Acta Crystallogr. **15**, 1311 (1962).
[27] D. Taupin, Bull. Soc. Fr. Mineral. **87**, 469 (1964).
[28] W. H. Zachariasen, *Theory of X-ray Diffraction in Crystals* (Wiley, New York, 1945).
[29] Near degeneracy, the diffusion constant varies with carrier density [1,19]; however, as the plasma diffuses it quickly reaches the low density limit.